



**HAL**  
open science

## Nanoscale organization of tetraspanins during HIV-1 budding by correlative dSTORM/AFM

Selma Dahmane, Christine Doucet, Antoine Le Gall, Célia Chamontin, Patrice Dosset, Florent Murcy, Laurent Fernandez, Desiree Salas, Eric Rubinstein, Marylène Mougel, et al.

► **To cite this version:**

Selma Dahmane, Christine Doucet, Antoine Le Gall, Célia Chamontin, Patrice Dosset, et al.. Nanoscale organization of tetraspanins during HIV-1 budding by correlative dSTORM/AFM. Nanoscale, 2019, 11, pp.6036 - 6044. 10.1039/c8nr07269h . hal-03103990v2

**HAL Id: hal-03103990**

**<https://hal.science/hal-03103990v2>**

Submitted on 25 Nov 2022

**HAL** is a multi-disciplinary open access archive for the deposit and dissemination of scientific research documents, whether they are published or not. The documents may come from teaching and research institutions in France or abroad, or from public or private research centers.

L'archive ouverte pluridisciplinaire **HAL**, est destinée au dépôt et à la diffusion de documents scientifiques de niveau recherche, publiés ou non, émanant des établissements d'enseignement et de recherche français ou étrangers, des laboratoires publics ou privés.

# Nanoscale organization of tetraspanins during HIV-1 budding by correlative dSTORM/AFM†

Cite this: DOI: 10.1039/c8nr07269h

Q2

Selma Dahmane,<sup>‡a</sup> Christine Doucet,<sup>‡a</sup> Antoine Le Gall,<sup>a</sup> Célia Chamontin,<sup>b</sup> Patrice Dosset,<sup>a</sup> Florent Murcy,<sup>a</sup> Laurent Fernandez,<sup>a</sup> Desirée Salas,<sup>a</sup> Eric Rubinstein,<sup>c,d</sup> Marylène Mougel,<sup>b</sup> Marcelo Nollmann<sup>a</sup> and Pierre-Emmanuel Milhiet<sup>ID</sup> <sup>\*,a</sup>

Membrane partition and remodeling play a key role in numerous cell mechanisms, especially in viral replication cycles where viruses subvert the plasma membrane to enter and escape from the host cell. Specifically assembly and release of HIV-1 particles require specific cellular components, which are recruited to the egress site by the viral protein Gag. We previously demonstrated that HIV-1 assembly alters both partitioning and dynamics of the tetraspanins CD9 and CD81, which are key players in many infectious processes, forming enriched areas where the virus buds. In this study we correlated super resolution microscopy mapping of tetraspanins with membrane topography delineated by atomic force microscopy (AFM) in Gag-expressing cells. We revealed that CD9 is specifically trapped within the nascent viral particles, especially at buds tips, suggesting that Gag mediates CD9 and CD81 depletion from the plasma membrane. In addition, we showed that CD9 is organized as small membrane assemblies of few tens of nanometers that can coalesce upon Gag expression.

Received 6th September 2018,  
Accepted 1st March 2019

DOI: 10.1039/c8nr07269h

rs.c.li/nanoscale

## Introduction

A common feature of living organisms is the presence of a lipid barrier delimiting cells. Yet this lipid membrane allows communication between the cell interior and its environment. This is mediated either by protein complexes embedded in the lipid bilayer, able to transduce signals, or by exchange of material through membrane vesicles. This latter phenomenon involves a sequence of membrane remodeling events, which include membrane deformation and lateral reorganization of membrane components. Indeed, the plasma membrane can be envisioned as a mosaic of micro and nano-domains of distinct lipid and protein compositions. These domains are dynamic and their lateral organization leads to specific local properties of the plasma membrane (recently reviewed in ref. 1 and 2). Remodeling of this organization is involved in numerous processes such as cellular adhesion, endo- and exocytosis, cell fusion or migration.

Viral cycles involve membrane remodeling during virus entry and egress, two critical steps for infection. In addition, these events are archetypes of coordinated reorganization of host membrane components and membrane deformation. Understanding their orchestration is thus of interest with respect to infectious mechanisms and membrane biology in general. In Human Immunodeficiency type 1 virus (HIV-1), viral egress is initiated by the structural protein Gag that is necessary and sufficient to release virus-like particles (VLPs).<sup>3</sup> Gag is expressed as a polyprotein that will be cleaved after particle release. Gag is targeted to the inner leaflet of the plasma membrane where it multimerizes, induces membrane curvature (budding sites) and finally membrane fission by recruiting host factors such as the ESCRT machinery.<sup>4</sup> Lipids of the host plasma membrane play a key role in this process.<sup>5</sup> Among these, sphingolipids and cholesterol<sup>6,7</sup> are known to form or be enriched in different types of microdomains that could behave as pre-formed recruitment platforms.<sup>6</sup> It was proposed that HIV-1 Gag proteins can sense cholesterol and acyl chain environment in membranes. HIV-1 also hijacks host proteins to achieve egress. This is the case of the ESCRT machinery, as already mentioned. But other proteins may be involved, amongst which proteins of the tetraspanin family.

Tetraspanins belong to a family of proteins characterized by four transmembrane regions and a specific fold in the larger of the 2 extracellular domains. All human cell types express several of these proteins which play an essential role in mul-

<sup>a</sup>Centre de Biochimie Structurale (CBS), INSERM, CNRS, Univ Montpellier, France.  
E-mail: pem@cbs.cnrs.fr

<sup>b</sup>IRIM, CNRS, University of Montpellier, Montpellier, France

<sup>c</sup>Inserm, U935, Villejuif, France

<sup>d</sup>Université Paris Sud, Institut André Lwoff, Villejuif, France

†Electronic supplementary information (ESI) available. See DOI: 10.1039/c8nr07269h

‡These two authors equally contributed to the work.

multiple cellular processes ranging from cell morphology, migration, cell–cell fusion and signaling.<sup>8</sup> Tetraspanins are molecular organizers within the plasma membrane forming a dynamic network of protein–protein interactions at the cell surface by interacting with one another and with other transmembrane proteins (integrins, immunoglobulin superfamily proteins and others).<sup>9–11</sup> This interaction network is referred to as the tetraspanin web or Tetraspanin-enriched microdomains (TEM).<sup>12</sup> A fraction of tetraspanins and associated proteins concentrate into microscopically visible structures named tetraspanin-enriched areas (TEA) or platforms.<sup>13,14</sup> Interestingly, single molecule microscopies have revealed that tetraspanins are also organized in dynamic nano-clusters.<sup>14–16</sup> How these two levels of organization participate in tetraspanin functions is not clear.

Several studies have shown colocalization of several tetraspanins (CD9, CD63, CD82 and CD81) with HIV-1 Gag and Env, in several cell types including T cells.<sup>17–19</sup> TEMs were thus proposed to constitute gateways for HIV-1 assembly and budding. More recently, we have demonstrated using single molecule tracking experiments that both CD9 and CD81 are specifically recruited and sequestered within Gag assembly sites. This supports that viral components do not cluster at pre-existing microdomains but rather promote the formation of distinct domains enriched in tetraspanins for the execution of specific functions, yet not fully elucidated.<sup>20</sup> Tetraspanin knockdown or inhibition by specific antibodies also revealed that tetraspanin down-regulation decreases virus entry and replication in macrophages.<sup>21,22</sup> In addition several studies pinpointed a potential role of tetraspanins in modulating HIV-1 infectivity through their incorporation into the released viral particles. Overexpression of tetraspanins in virus-producing cells led to the production of virions with less infectivity.<sup>23,24</sup> The presence of these proteins at exit sites also reduced the formation of syncytia in virus-producing cells and cell-to-cell fusion induced by the virus.<sup>23,25,26</sup> Conversely, CD81 and CD82 levels are down-regulated by the HIV-1 accessory proteins Vpu and Nef, which induce protein sequestration in intra-cellular compartments and degradation, leading to decreased levels at the plasma membrane.<sup>27</sup> These observations raise important questions concerning the role of CD9 and CD81 in the different steps of viral replication, from Gag recruitment at the plasma membrane to budding and release of viral particles. In particular, although CD9 and CD81 are involved in many membrane remodeling events,<sup>28</sup> it is not clear whether they could play a role in membrane deformation and/or fission during HIV-1 egress. In addition, characterizing the effect of Gag on tetraspanin organization may help understand the relative importance of the micro- and nanoscale organization of the tetraspanin web.

Here we developed and used correlative microscopy combining dSTORM (direct stochastic optical reconstruction microscopy) with AFM (atomic force microscopy),<sup>29</sup> two advanced microscopy techniques allowing lateral resolution of a few tens of nanometers, well beyond light diffraction law. Membrane topography including budding sites was delineated

by the AFM (for a recent review, see ~~ref.~~<sup>30</sup>) whereas CD9 mapping was analyzed using dSTORM, a type of SMLM based on photoswitching of fluorophores.<sup>31,32</sup> Our results show that (i) Gag expression induces the concentration of CD9 and CD81 nanoclusters within Gag assembly sites. While the distribution of these clusters is dramatically altered, their intrinsic nanoscale structure does not change much upon Gag expression; (ii) CD9 concentrates within nascent viral particles. In most cases, it localizes at the very tip of viral buds and is excluded from the bases of the budding sites. This supports a role in membrane curvature induction or sensing rather than fission; (iii) Gag mediates specific depletion of both CD9 and CD81 from cell surface, suggesting that CD9 and CD81 depletion is due to their accumulation in Gag-induced VLP budding sites. This happens even in the absence of the regulatory proteins Vpu and Nef and probably depends on VLPs release. Beyond the fields of tetraspanin and infection, this study demonstrates that this type of correlative microscopy is an incredible asset to depict at the nanoscale tight coordination between protein distribution/recruitment and membrane remodeling.

## Results

### Nanoscale organization of CD9 during Gag assembly

We had previously studied the dynamics of CD9 at the plasma membrane by Single Particle Tracking. Most CD9 harbors Brownian motion with proteins that sometimes can be transiently confined within tetraspanin-enriched areas.<sup>14</sup> In striking contrast, CD9 gets permanently trapped within HIV-1 assembly sites in cells expressing Gag.<sup>20</sup> This suggests that Gag interferes with CD9 interacting network. Yet how this affects CD9 nanoscale organization is not clear. To investigate this we performed dSTORM experiments under TIRF illumination to compare CD9 distribution in control and Gag-expressing HeLa cells. Cells were transfected with equimolar ratios of pGag and pGag-GFP, inducing the biosynthesis of VLPs mimicking HIV-1 infection<sup>33</sup> and stained with anti-CD9 antibodies labelled with Alexa647 24 h or 48 h after transfection. Importantly, imaging was performed in fixed cells since tetraspanins are very dynamic.<sup>9</sup> The localization precision was below 30 nm (Fig. S1A†).<sup>34</sup> dSTORM images of non-transfected HeLa cells showed a sparse distribution of CD9 molecules on the basal membrane surface (Fig. 1A, left column). The mean density of CD9 localizations (*i.e.* detected events) in control cells was  $1192 \mu\text{m}^2 \pm 127$  (sem) (Fig. 1B and Table S1†). Upon Gag expression (Fig. 1A, second and third columns and Fig. S1B†), we were able to identify individual puncta-like clusters membrane assemblies of Gag-GFP localized at the plasma membrane (white), consistent with previous reports. We found that CD9 partitioned into Gag-enriched areas and that the recruitment of CD9 at the Gag-GFP assembly sites induces a global modification in its spatial organization relative to Gag-GFP expressing and control HeLa cells (Fig. 1A). The mean density of localizations in cells 24 h and 48 h after transfection with

30 as  
supersc  
ript

5

10

15

20

25

30

35

40

45

50

55

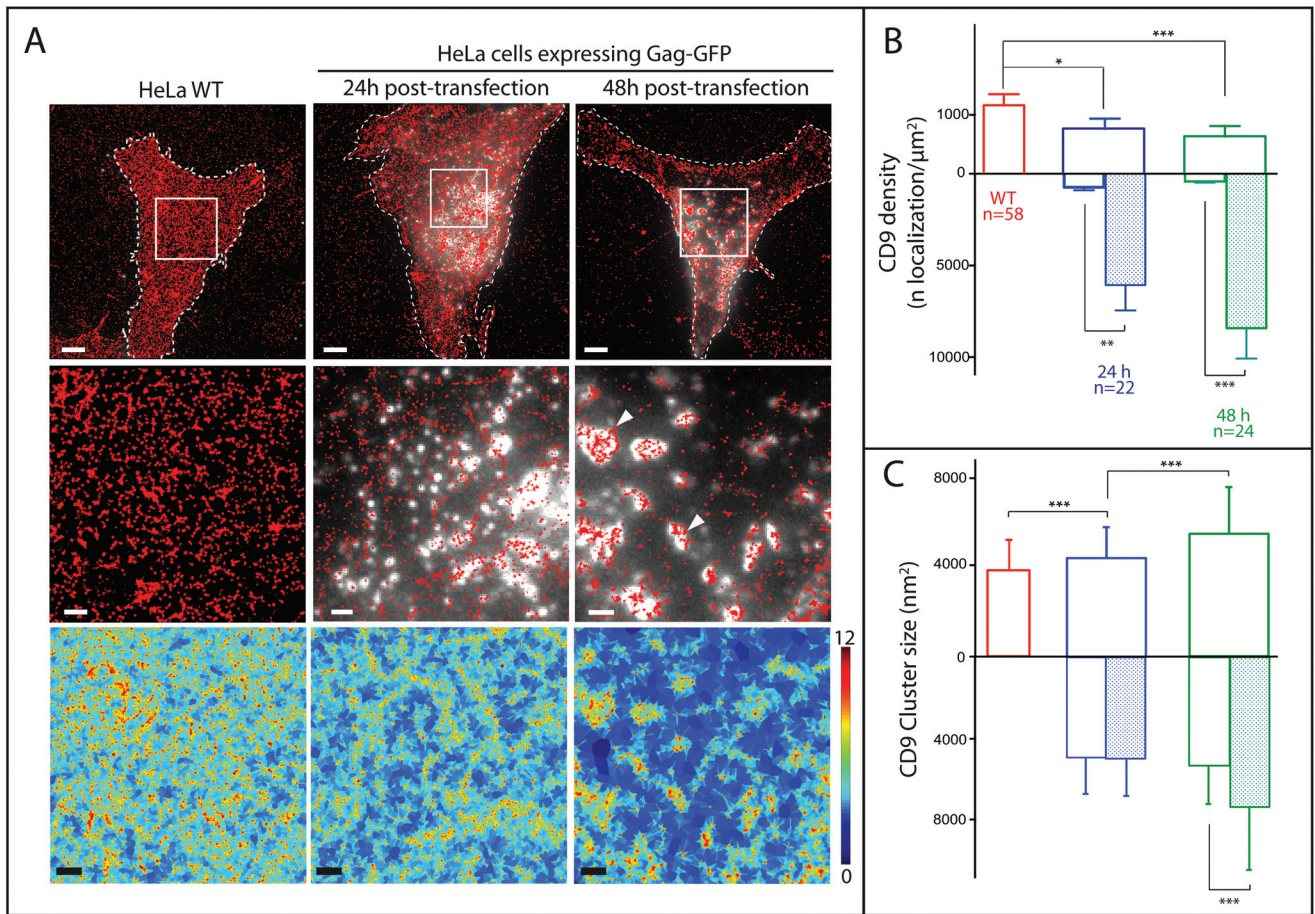


**Fig. 1** Gag proteins recruit and reorganize the tetraspanin CD9 at the plasma membrane. (A) Raw CD9 dSTORM localizations (red dots, 2 first rows) and local density map obtained from the SR-Tesseler framework (third row; the colour scale represents local densities in logarithmic scale) in HeLa cells expressing HIV-1 Gag-GFP (white signal in micrographs). From left to right: control cells; cells expressing Gag-GFP for 24 h or 48 h; the middle row show zoomed areas outlined in the upper images. Scale bars are 5  $\mu\text{m}$  (upper row) and 1  $\mu\text{m}$  (bottom rows); cells boundaries are shown with white dashed line. (B) dSTORM analysis. CD9 density (number of localization per  $\mu\text{m}^2$ ) in control cells (red) or in cells expressing Gag-GFP proteins 24 h (blue) or 48 h (green) after transfection. In the mirror histograms below the X axis, empty and hatched histograms represent the density outside and within Gag-GFP positive areas, respectively. Error bars are SEM and n is the number of analyzed cells. \*, \*\* and \*\*\* indicate p values below 0.05, 0.001 and 0.0001 respectively, as determined by the Mann–Whitney U-test (for exact p values, see Table S1†); (C) histograms of size distribution of CD9 clusters in  $\text{nm}^2$  for the 3 conditions. The legend is similar to B.

pGag-GFP decreased to  $793 \pm 141$  and  $658 \pm 151$  per  $\mu\text{m}^2$ , indicating a reduction in CD9 levels upon Gag expression. Interestingly, using a mask based on Gag-GFP signal, we noted a dramatic increase in the localization density within Gag-GFP-enriched areas at the cost of surrounding areas ( $8430 \pm 1655$  versus  $428 \pm 63$  localizations per  $\mu\text{m}^2$  in areas devoid of Gag, 48 h after transfection) (Fig. 1B and Table S1†). As expected from Fig. 1A, CD9 localization density in Gag-GFP foci was correlated to Gag-GFP intensity (Fig. S1C, Fig. S1D, and Table S4† for Kendall's tau correlation coefficients).

To refine our analysis of CD9 lateral reorganization, single molecule localizations were analyzed using a segmentation procedure based on Voronoï diagrams. This method allows a precise and automatic segmentation and quantification of protein organization (Fig. 1A). A framework named “SR-Tesseler”<sup>35</sup> was used to estimate the size (in  $\text{nm}^2$ ) of CD9 clusters at the plasma membrane (for more details, see the

ESI†). In control cells, the mean area of CD9 clusters or assemblies was  $3710 \pm 1513$   $\text{nm}^2$  (Fig. 1C and Table S2†) that corresponds to a disk of 69 nm diameter. A significant increase of this mean area was observed upon Gag expression, up to  $5471 \pm 2198$   $\text{nm}^2$  for cells analyzed 48 h after transfection that corresponds to a disk of 83 nm diameter. This increase was even more pronounced when considering only Gag-enriched areas using the mask method described above:  $6527 \pm 2763$   $\text{nm}^2$  for cells 48 h post-transfection versus  $3710 \pm 1513$   $\text{nm}^2$  for control cells, corresponding to a disk of 91 nm diameter (see Table S2† and the mirror histograms in Fig. 1C). Gag expression thus induces an enlargement of CD9 nanodomains, supporting that Gag modulates CD9 interacting network. However the increase in CD9 cluster sizes remains moderate, even in areas of very high CD9 density such as Gag assembly sites. Interestingly, 70–90 nm diameter is smaller than the size range of HIV-1 budding sites.<sup>36</sup> This suggests

that CD9 may be confined within the budding sites. To verify this, we wanted to precisely correlate CD9 localization with the topography of Gag-induced budding sites.

### Correlation between Gag assembly within VLP buds and CD9 dSTORM

We first implemented correlative TIRF and AFM imaging. To ensure that apical cellular membranes imaged by AFM were in the TIRF evanescent field, we focused on thin regions present at the cell periphery (Fig. 2). Topographic images of the cell surface revealed membrane protrusions that overlapped with Gag-GFP foci, suggesting they were VLPs. Some fluorescent areas did not coincide with membrane protrusion, likely because Gag assembly occurred on the basal membrane not accessible to the AFM tip (see the asterisk in Fig. 2). Virus-like buds were on average  $104 \pm 49$  nm high and  $162 \pm 75$  nm wide, which is in accordance with measurements derived from super resolution microscopy (see the review<sup>36</sup> or electron microscopy studies<sup>37</sup>). As expected the size distribution of virus-like buds was heterogeneous (Fig. S2A†), reflecting the progression of the budding process. As a matter of fact, the surface of buds measured by AFM correlates with Gag-GFP content (Fig. 2E). In addition, AFM allowed further characterization of VLPs formation as shown in Fig. 2F where the AFM tip could delineate

2 budding sites that cannot be differentiated with conventional TIRF microscopy. This illustrates well the gain in resolution obtained by AFM.

We thus combined dSTORM and AFM on cells expressing Gag-GFP to get more details on CD9 organization in Gag-enriched domains (Fig. 3). CD9 clusters characterized by dSTORM overlapped well with the shape of Gag-GFP budding sites delineated by the AFM tip (Fig. 3A–D). In advanced buds (spherical bud attached to the membrane by a neck), the neck area was devoid of CD9 (*e.g.* Fig. 3C). In nascent buds CD9 was localized at the very tip of membrane protrusions and mostly excluded from the basis of budding sites (Fig. 3F and Fig. S3†). Exclusion from the neck region was quantified by measuring CD9 density at varying distances from the plasma membrane to the bud tip (number of localizations per  $\mu\text{m}^2$ ) (Fig. S3B and see ESI† for details). Regions close to the tip harbored higher CD9 densities. This demonstrates that CD9 is indeed trapped within the nascent bud. Moreover, CD9 seems to preferentially associate with membrane regions of high positive curvature. As described in Fig. 1, some CD9 clusters were also observed in membrane areas devoid of Gag-GFP proteins. Since calculation of CD9 densities from 2D projected areas (as in Fig. 1) may have introduced a drawback, especially in buds, we calculated the number of CD9 localizations

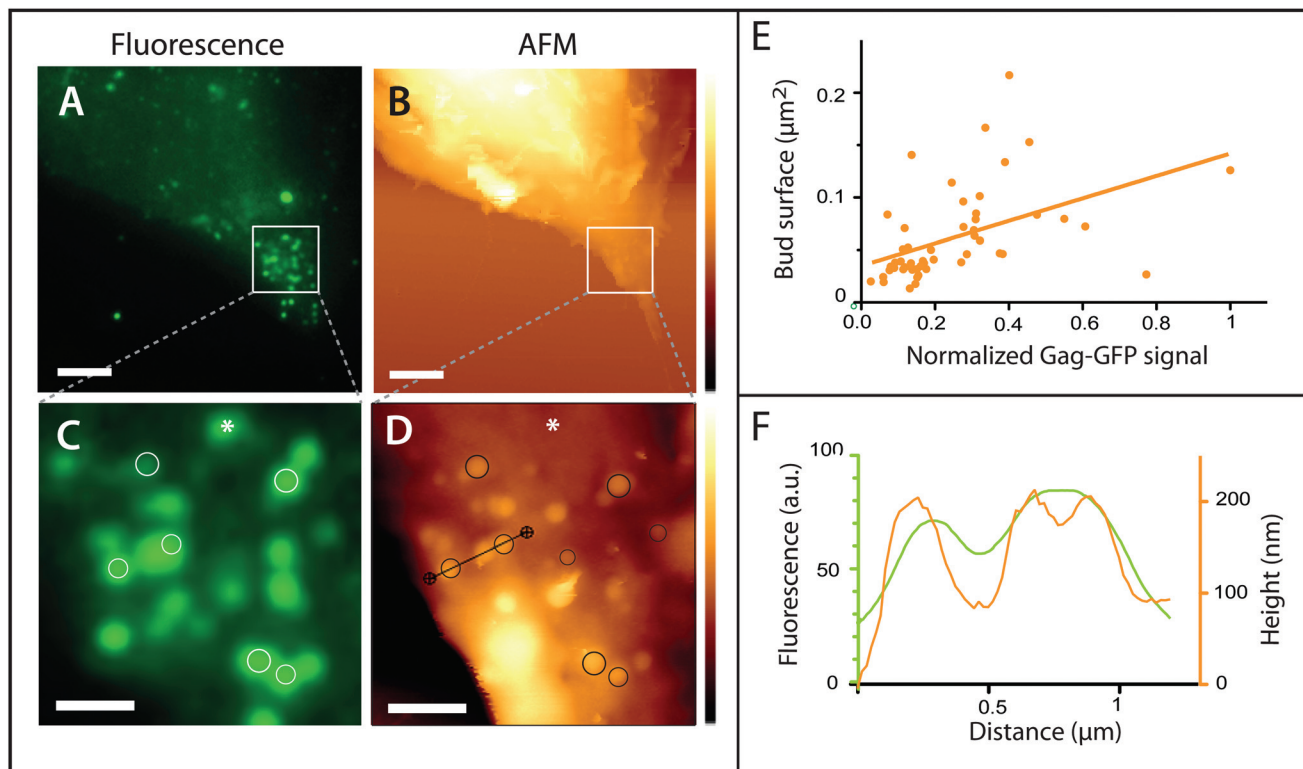


**Fig. 2** Nanoscale imaging of HeLa cells expressing Gag-GFP using correlated fluorescence-atomic force microscopy. Gag-GFP fluorescence image (A and C) and AFM topographic images (B and D) were compared (48 h post-transfection here). The circles highlight some correlation between fluorescence and the membrane protrusion delineated by the AFM tip. The asterisk points out a Gag assembly where no membrane protrusion was observed by AFM. (E) Normalized Gag-GFP signal as a function of the bud surface measured by AFM ( $R^2 = 0.22$ ). Data were collected from 5 different cells. (F) Profile plot of the topography (orange line) and fluorescence signal (green line) along the section indicated by the black line on the AFM image. Scale bars are 5 (A and B) or 1  $\mu\text{m}$  (C and D). The AFM z colour scales are 6.6  $\mu\text{m}$  (upper AFM image) and 800 nm (lower image).

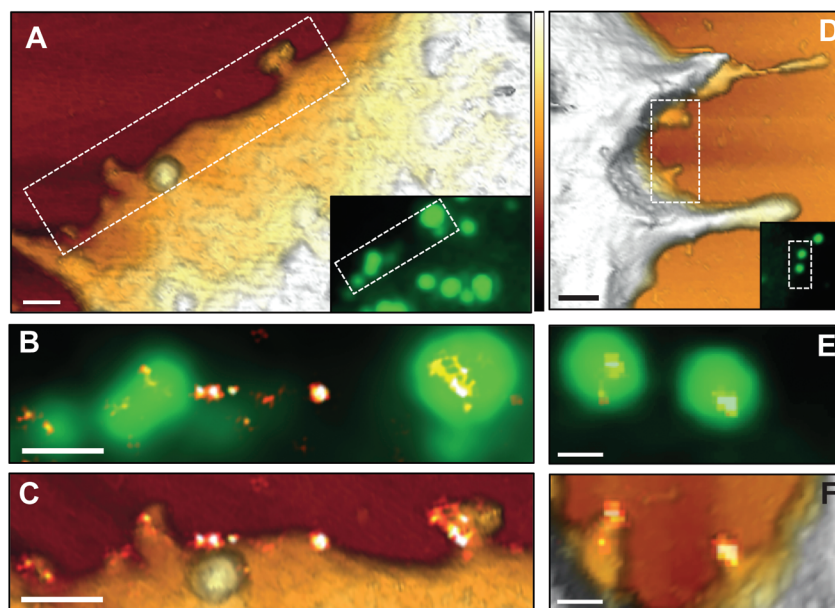


**Fig. 3** CD9 recruitment at HIV-1 budding sites. HeLa cells expressing HIV-1 Gag-GFP were immuno-stained with anti-CD9 coupled to Alexa-647 and imaged by AFM (first row), conventional fluorescence (second row) and dSTORM (third row): images of two different cells (the dotted line delineates the zoomed areas shown below and the insets are the corresponding Gag-GFP signal fluorescence images); B and (E) overlays of the Gag-GFP picture with the reconstructed dSTORM image of the tetraspanin CD9. Scale bars are 500 nm (A and D) or 200 nm (B, C, E and F). The colour z scale shown in A and D is 300 nm.

divided by the membrane area extracted from AFM images (see ESI†). Taking into account the membrane topography, we confirmed that CD9 density is higher in Gag-GFP budding sites ( $3836 \pm 934$  localizations per  $\mu\text{m}^2$ ) compared to membrane regions where Gag proteins are absent ( $505 \pm 111$ ) (Fig. S2B†). The areas measured by AFM may be slightly overestimated due to tip convolution, leading to a slight underestimation of CD9 density. Importantly, despite this potential bias we still observe a strong increase of CD9 density within nascent buds.

#### Gag reduces the cell surface expression of both tetraspanins CD9 and CD81

Interestingly, quantification of our dSTORM data suggests that CD9 level at the plasma membrane globally decreased when Gag is expressed. To confirm this, we analyzed cell surface expression of both CD9 and CD81 on HeLa cells expressing or not Gag-GFP using FACS. Cells were then fixed and stained with anti-CD9 or anti-CD81. 30–40% of cells were positively transfected and we defined 3 types of populations: untransfected cells (GFP–) and cells with intermediate (GFP+) or high (GFP++) levels of expression (Fig. 4A). While GFP-transfected cells had comparable CD9 levels in the 3 populations, CD9 surface levels were decreased by 70–80% in cells strongly expressing Gag-GFP, as compared to GFP-negative cells from the same sample. Intra-sample ratios of CD9 and CD81 levels in GFP++ or GFP+ versus GFP– cells were averaged from 4 independent experiments (Fig. 4B). The values confirmed that cells with high Gag expression are depleted of CD9 and CD81. In contrast, we found that the cell surface levels of CD46, a non-

raft transmembrane protein with little association with tetraspanins, was weakly affected upon overexpression of Gag proteins (Fig. 4), indicating that Gag specifically affects CD9 and CD81 surface levels. These levels are known to be down-regulated in an HIV-1 infection context due to their degradation and intracellular sequestration by the viral proteins Vpu and Nef.<sup>27</sup> We wondered if CD9 and CD81 surface levels were decreased because of protein internalization. For this, we immuno-stained CD9 and CD81 in permeabilized cells expressing Gag. No intracellular signal was detected (Fig. S4†). The fact that CD9 and CD81 are strongly concentrated at the tip of the buds suggests that their downregulation at the cell surface is due to tetraspanin escape from the plasma membrane when VLPs are released (model presented in Fig. 5). The lateral reorganization of tetraspanins by Gag thus has nanoscopic as well as macroscopic consequences. As of now, the impact of this depletion on the viral cycle and/or the host cell fate is not clear. However, we confirmed that depletion of CD9 and/or CD81 from HeLa cells by siRNA did not affect VLPs release (Fig. S4A and B†). But interestingly, we noted a compensation effect: CD9 is more concentrated in VLPs when CD81 is depleted, and the reverse is also true. This suggests that Gag induces an overall tetraspanin concentration in VLPs during viral egress.

## Discussion

Tetraspanins have been described as organizers of the plasma membrane of eukaryotic cells, playing a key role in membrane

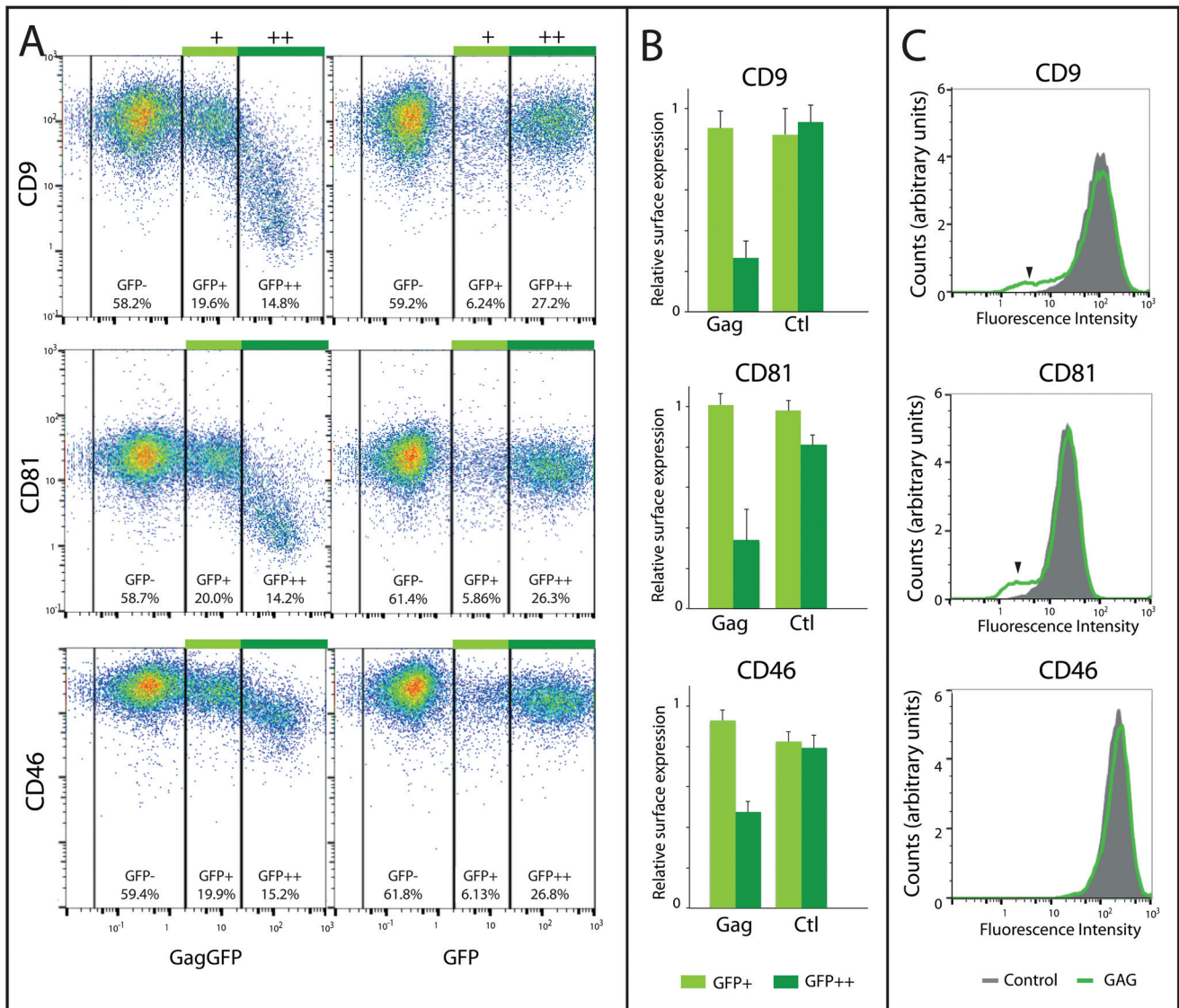


**Fig. 4** Gag reduces tetraspanin levels at the cell surface of HeLa cells. (A, B and C) Surface expression of CD9, CD81 and CD46 measured by flow cytometry 48 h after transfection with Gag-GFP or GFP (control). (A) Representative flow cytometry 2D dot plots of gated living cells; three cell populations were defined based on their GFP intensity (GFP-, GFP+ and GFP++). Percentages indicate the representative fraction of each population; (B) mean CD9, CD81 and CD46 levels were quantified for each population and normalized to GFP- levels. Data were averaged from 3 independent experiments. Error bars are standard deviations. (C) Surface levels of CD9, CD81 and CD46 in HeLa cells transfected with GFP alone (grey) or with Gag-GFP (green line). Black arrowheads indicate HeLa cells with CD9 or CD81 depletion.

remodeling especially in the infection context. In this study we used dSTORM/AFM correlative microscopy to investigate how HIV-1 Gag affects the lateral organization of the CD9 tetraspanin that becomes trapped within the viral particle.

We characterized CD9 localization in control cells using dSTORM and reported a clustered organization. Other tetraspanins have been previously characterized by high-resolution techniques, namely STED<sup>16</sup> and dSTORM.<sup>15,38</sup> Interestingly, their localizations were also clustered, yet with slightly larger sizes (100–150 nm wide) than found here for CD9 (67 nm). However, even though CD9 transiently associates with the tetraspanins characterized in these studies (*e.g.* CD82, CD81, CD53), their distribution is not expected to be identical. In

fact, the area of CD81 clusters measured in the present work was slightly larger than that of CD9 (disk of 81 nm diameter, Fig. S6†). This difference fits well with the slower diffusion of CD81 compared to CD9, as measured by single molecule tracking.<sup>39</sup> In addition, it is probable that the tetraspanin clusters differ in composition and size from one cell to another. Taken together, cluster sizes measured in the publications cited above fall in the same range and support a model whereby tetraspanins diffuse in the plasma membrane, embedded in small assemblies that could contain other tetraspanins, some protein partners, and lipids.<sup>9,16</sup>

CD9 and CD81 being recruited at budding sites during HIV-1 egress suggested that functional platforms could orig-

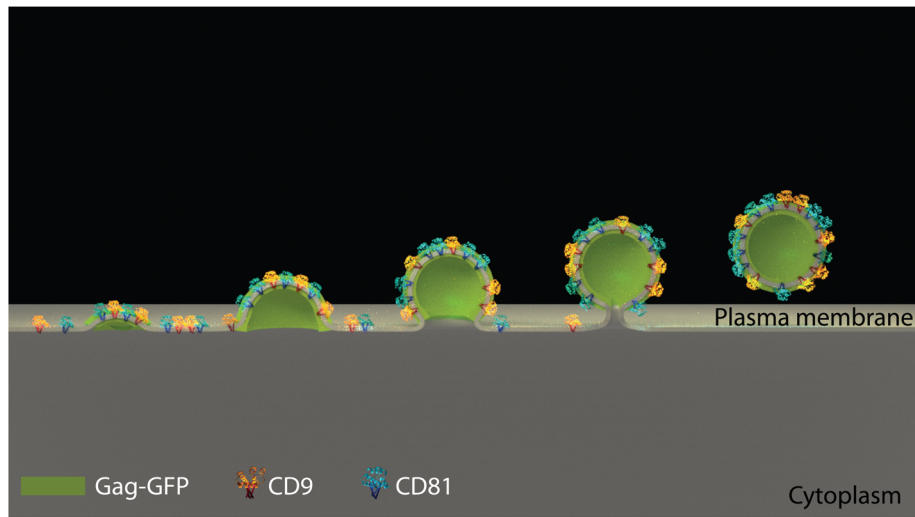


**Fig. 5** Model of tetraspanin lateral organization in the HIV-1 context. This scheme represents how the tetraspanins CD9 and CD81 (in blue and yellow) are laterally segregated within Gag-induced budding sites (in green). This leads to decreased CD9 and CD81 levels in the surrounding plasma membrane (in light grey), resulting in a net protein loss when virus-like particles are excised.

inate from the gathering of these small assemblies. Indeed we confirm here that, upon expression of Gag-GFP in a model system recapitulating HIV-1-induced VLP production, CD9 and CD81 lateral organization is dramatically changed (respectively Fig. 1 and Fig. S6A†) and the two tetraspanins are highly concentrated in regions of Gag assembly, forming large tetraspanin-enriched areas. Surprisingly the average cluster size did not radically change upon Gag expression (Fig. 1C and Fig. S6B†), suggesting that the large CD9 and CD81 assemblies observed in Gag-enriched areas are composed of tetraspanin clusters that gather but do not fully coalesce (they can be resolved by dSTORM). This local concentration of tetraspanins is compensated by a decrease in their density in surrounding regions (as compared to control cells, Fig. S1E†), indicating that CD9 enrichment in Gag<sup>+</sup> areas is due to lateral reorganization of CD9 rather than protein recruitment from intracellular compartments. This model is in good agreement with our previous work showing that CD9, which diffuses in a Brownian motion in the plasma membrane, is trapped within Gag assembly sites.<sup>20</sup> Gag is most likely the driving force that concentrates tetraspanin clusters, which probably co-segregate with other membrane partners that could facilitate budding. As previously suggested, lipid composition of these membrane assemblies could also play a key role in building large membrane platforms since Gag proteins are recruited by PIP2 lipids in a cholesterol-dependent manner.<sup>6,40</sup>

Correlative dSTORM/AFM on cells expressing Gag-GFP showed that CD9 concentrates at the very tip of nascent VLPs with almost complete exclusion from buds necks at late stages. CD81 had previously been observed mainly localized at the tips of elongated Influenza viruses using EM.<sup>41</sup> In this particular case, CD81 was proposed to also play a role in fission due to its presence at both ends, including the side attached to the host cell. This is quite different from our observations with

CD9, which is thus most likely not involved in bud scission. But CD9 seems to have the propensity to partition within positively curved membranes. This is in good agreement with the presence of CD9 and CD81 in tubular structures such as membrane protrusions and filipodia (data not shown and [ref. 42](#)).<sup>42 in superscript</sup> The correlation between CD9 density and membrane curvature could either reflect a role of CD9 in membrane remodeling and deformation, especially positive curvature, or its sensitivity to membrane curvature. At that time it is difficult to discriminate between these two models but the first hypothesis is more likely since we have also observed CD9 and CD81 in flat membranes. It is then more tempting to speculate that these proteins are important in the formation of highly curved membranes encountered during virus budding, in the production of exosomes from multivesicular bodies,<sup>43</sup> as well as in cell fusion process observed during the gamete fusion where association of CD9 with high membrane curvature regions has been reported previously in oocytes<sup>44</sup> or during myoblast fusion.<sup>45</sup> Interestingly, protein confinement within membrane domains has been proposed to induce bending of the lipid bilayer, even in the absence of any specific protein functional domain.<sup>46,47</sup> Importantly, the smaller the protein, the stronger the effect.<sup>46</sup> These observations are particularly interesting regarding tetraspanins: indeed, they are small proteins (~20 kDa) and they are transiently or permanently confined within molecular platforms at the plasma membrane (reviewed in [ref. 39](#)).<sup>39 in superscript</sup> In this regard, modulation of their confinement through interacting partners (in the case of this study, by Gag) could mediate their ability to curve membranes.

We then performed single or dual depletion of CD9 and CD81 in HeLa cells and measured VLP production (Fig. S5A and B†). Similarly to what has already been described,<sup>23</sup> CD9 and CD81 are not essential for VLPs release in HeLa cells. However, we observed that CD9 silencing led to an increase of

CD81 expression within VLPs, and *vice versa*, suggesting that one tetraspanin could compensate for the loss of another. Interestingly, this effect was not observed in cell extracts, emphasizing a specific role of tetraspanins in viral particles. The other side of the coin of this redundancy is the difficulty to clearly establish their functional role.

Markus Thali's group has demonstrated that, despite their enrichment at viral exit sites, the overall levels of tetraspanins are decreased in HIV-1-infected cells. More specifically CD81 down-regulation in HIV-1 infected cells was explained by its degradation in proteasomal and lysosomal pathways. These processes were shown to depend upon HIV proteins Vpu and Nef.<sup>27</sup> Here, we report that Gag-GFP expression could also trigger CD9 and CD81 depletion in the absence of Vpu and Nef. Given the high concentration of CD9 and CD81 within Gag-induced buds, we propose that their depletion is directly linked to VLP release from host cells. Even if the fraction of cellular plasma membrane escaping through this process remains low (as assessed by unaffected levels of CD46), CD9 and CD81 global protein levels are impacted most probably because of their high concentration within Gag assembly sites. Interestingly, tetraspanin levels influence HIV-1 life cycle at different stages and in opposite manners. Indeed, CD81 potentiates HIV-1 transcription<sup>22,45</sup> through its association to SAMHD1,<sup>46</sup> while overexpression of tetraspanins at the surface of virions, including CD9 and CD81, decrease their infectivity.<sup>23,24</sup> Tetraspanins thus appear as key elements in the modulation of HIV-1 virulence. Moreover, membrane excision could also have an impact on other membrane components that are highly enriched within VLPs, such as cholesterol or PIP2 for instance.<sup>40</sup>

Taken together our results shed new light on the involvement of CD9 and CD81 during HIV-1 egress using a new type of correlative microscopy that is suitable to investigate virus-host interactions, providing topographic details and molecular mapping at the nanoscale in native conditions. Of note, the cellular model we used is widely accepted for the study of HIV-1 assembly (e.g. ~~ref.~~ 50–52). For instance, the cellular ESCRT machinery necessary for HIV assembly has been extensively studied and demonstrated as functional in these cells<sup>53</sup> and our previous study of the role of the tetraspanins in HIV assembly<sup>20</sup> has been already conducted in HeLa cells. Moreover, correlative AFM/STORM relies on the possibility to image thin regions of cells where the apical membrane (accessible to AFM) lies in the evanescent TIRF field. HeLa cells, which are adherent, are thus an ideal compromise for such studies. Nevertheless, we think that our results are transposable to T cells or DCs, as tetraspanins are ubiquitous proteins. The acute description of tetraspanin distribution at a nanoscopic and microscopic scale in the 3D topography landscape probed by AFM allow us to make new hypotheses regarding tetraspanins functions in membrane bending. More generally such correlative microscopy appears as an outstanding technique to analyze membrane remodeling and protein partitioning in critical biological processes.

## Author contributions

Conceptualization, M. N. & P. E. M.; Methodology, S. D., A. L. G., C. D. & P. D.; Validation, S. D., C. D., M. M., M. N. & P. E. M.; Formal analysis; S. D., C. D., A. L. G. & P. E. M.; Investigation, S. D., C. D., C. C., F. M., L. F. & D. S. P.; Resources, M. M., E. R. and P. E. M.; Writing - Original Draft, S. D., C. D. & P. E. M.; Writing - Review & Editing, C. D. E. R., M. N. & P. E. M.; Visualization, C. D. & P. E. M.; Supervision, M. M., M. N. & P. E. M.; Funding acquisition, M. N. & P. E. M.

## Conflicts of interest

There are no conflicts to declare.

## Acknowledgements

We acknowledge the support from France-BioImaging (FBI, ANR-10-INSB-04), the French Infrastructure for Integrated Structural Biology (FRISBI, ANR-10-INBS-05), the European Research Council Starting (ERC-Stg-260787), the Agence Nationale pour la Recherche (ANR-15-CE11-0023) and the GIS IBISA (Infrastructures en Biologie Santé et Agronomie). LF and DSP were recipients of the French Ministry of Education and Research. LF was a FRM fellow and SD salary was paid with a Sanofi-Pasteur contract. We are grateful to Zhanna Santybayeva for creating the cartoon in Fig. 5, Markus Thali for providing the Gag-GFP plasmids, and Heiko Haschke (~~HPK company~~) for his technical help and helpful discussion. Bruker Nano Surfaces

## References

- 1 K. Raghunathan and A. K. Kenworthy, *Biochim. Biophys. Acta, Biomembr.*, 2018, **1860**, 2018–2031.
- 2 D. Krapf, *Curr. Opin. Cell Biol.*, 2018, **53**, 15–21.
- 3 L.-A. Carlson, J. A. G. Briggs, B. Glass, J. D. Riches, M. N. Simon, M. C. Johnson, B. Müller, K. Grünwald and H.-G. Kräusslich, *Cell Host Microbe*, 2008, **4**, 592–599.
- 4 J. R. Lingappa, J. C. Reed, M. Tanaka, K. Chutiraka and B. A. Robinson, *Virus Res.*, 2014, **193**, 89–107.
- 5 J. Fantini, D. Hammache, G. Piéroni and N. Yahi, *Glycoconjugate J.*, 2000, **17**, 199–204.
- 6 A. Ono, *Vaccine*, 2010, **28**(Suppl 2), B55–B59.
- 7 A. A. Waheed and E. O. Freed, *Virus Res.*, 2009, **143**, 162–176.
- 8 S. Charrin, S. Jouannet, C. Boucheix and E. Rubinstein, *J. Cell Sci.*, 2014, **127**, 3641–3648.
- 9 S. Charrin, F. cois Le Naour, O. Silvie, P. E. Milhiet, C. Boucheix and E. Rubinstein, *Biochem. J.*, 2009, **420**, 133–154.
- 10 M. E. Hemler, *Nat. Rev. Mol. Cell Biol.*, 2005, **6**, 801–811.
- 11 S. Levy and T. Shoham, *Physiology*, 2005, **20**, 218–224.
- 12 F. Berditchevski, *J. Cell Sci.*, 2001, **114**, 4143–4151.

- 1 13 O. Barreiro, M. Zamai, M. Yanez-Mo, E. Tejera, P. Lopez-Romero, P. N. Monk, E. Gratton, V. R. Caiolfa and F. Sanchez-Madrid, *J. Cell Biol.*, 2008, **183**, 527–542.
- 5 14 C. Espenel, E. Margeat, P. Dosset, C. Arduise, C. Le Grimellec, C. A. Royer, C. Boucheix, E. Rubinstein and P.-E. Milhiet, *J. Cell Biol.*, 2008, **182**, 765–776.
- 10 15 C. M. Termini, M. L. Cotter, K. D. Marjon, T. Buranda, K. A. Lidke and J. M. Gillette, *Mol. Biol. Cell*, 2014, **25**, 1560–1573.
- 16 M. Zuidscherwoude, F. Göttfert, V. M. E. Dunlock, C. G. Figdor, G. van den Bogaart and A. B. van Spriel, *Sci. Rep.*, 2015, **5**, 12201.
- 17 B. Grigorov, V. Attuail-Audenis, F. Perugi, M. Nedelec, S. Watson, C. Pique, J.-L. Darlix, H. Conjeaud and D. Muriaux, *Retrovirology*, 2009, **6**, 28.
- 15 18 C. Jolly and Q. J. Sattentau, *J. Virol.*, 2007, **81**, 7873–7884.
- 19 S. Nydegger, *J. Cell Biol.*, 2006, **173**, 795–807.
- 20 20 D. N. Kremmentsov, P. Rassam, E. Margeat, N. H. Roy, J. Schneider-Schaulies, P.-E. Milhiet and M. Thali, *Traffic*, 2010, **11**, 1401–1414.
- 21 J. J. von Lindern, D. Rojo, K. Grovit-Ferbas, C. Yeramian, C. Deng, G. Herbein, M. R. Ferguson, T. C. Pappas, J. M. Decker, A. Singh, R. G. Collman and W. A. O'Brien, *J. Virol.*, 2003, **77**, 3624–3633.
- 25 22 E. Tippett, P. U. Cameron, M. Marsh and S. M. Crowe, *J. Leukocyte Biol.*, 2013, **93**, 913–920.
- 23 D. N. Kremmentsov, J. Weng, M. Lambele, N. H. Roy and M. Thali, *Retrovirology*, 2009, **6**, 64.
- 30 24 K. Sato, J. Aoki, N. Misawa, E. Daikoku, K. Sano, Y. Tanaka and Y. Koyanagi, *J. Virol.*, 2008, **82**, 1021–1033.
- 25 M. Gordón-Alonso, M. Yáñez-Mó, O. Barreiro, S. Alvarez, M. A. Muñoz-Fernández, A. Valenzuela-Fernández and F. Sánchez-Madrid, *J. Immunol.*, 2006, **177**, 5129–5137.
- 35 26 J. Weng, D. N. Kremmentsov, S. Khurana, N. H. Roy and M. Thali, *J. Virol.*, 2009, **83**, 7467–7474.
- 27 M. Lambelé, H. Koppensteiner, M. Symeonides, N. H. Roy, J. Chan, M. Schindler and M. Thali, *J. Virol.*, 2015, **89**, 3247–3255.
- 40 28 M. Fanaei, P. N. Monk and L. J. Partridge, *Biochem. Soc. Trans.*, 2011, **39**, 524–528.
- 29 P. D. Odermatt, A. Shivanandan, H. Deschout, R. Jankele, A. P. Nievergelt, L. Feletti, M. W. Davidson, A. Radenovic and G. E. Fantner, *Nano Lett.*, 2015, **15**, 4896–4904.
- 45 30 Y. F. Dufrêne, T. Ando, R. Garcia, D. Alsteens, D. Martinez-Martin, A. Engel, C. Gerber and D. J. Müller, *Nat. Nanotechnol.*, 2017, **12**, 295–307.
- 31 M. J. Rust, M. Bates and X. Zhuang, *Nat. Methods*, 2006, **3**, 793–795.
- 50 32 M. Heilemann, S. Van De Linde, M. Schüttpelz, R. Kasper, B. Seefeldt, A. Mukherjee, P. Tinnefeld and M. Sauer, *Angew. Chem., Int. Ed.*, 2008, **47**, 6172–6176.
- 33 S. Nydegger, M. Foti, A. Derdowski, P. Spearman and M. Thali, *Traffic*, 2003, **4**, 902–910.
- 34 D. I. Cattoni, A. M. Cardozo Gizzi, M. Georgieva, M. Di Stefano, A. Valeri, D. Chamoussset, C. Houbbron, S. Déjardin, J.-B. Fiche, I. González, J.-M. Chang, T. Sexton, M. A. Marti-Renom, F. Bantignies, G. Cavalli and M. Nollmann, *Nat. Commun.*, 2017, **8**, 1753.
- 5 35 F. Levet, E. Hosy, A. Kechkar, C. Butler, A. Beghin, D. Choquet and J.-B. Sibarita, *Nat. Methods*, 2015, **12**, 1065–1071.
- 36 B. Müller and M. Heilemann, *Trends Microbiol.*, 2013, **21**, 522–533.
- 10 37 J. A. G. Briggs, J. D. Riches, B. Glass, V. Bartonova, G. Zanetti and H.-G. Kräusslich, *Proc. Natl. Acad. Sci. U. S. A.*, 2009, **106**, 11090–11095.
- 38 K. D. Marjon, C. M. Termini, K. L. Karlen, C. Saito-Reis, C. E. Soria, K. A. Lidke and J. M. Gillette, *Oncogene*, 2016, **35**, 4132–4140.
- 15 39 S. Dahmane, E. Rubinstein and P.-E. Milhiet, *Viruses*, 2014, **6**, 1992–2011.
- 40 40 A. Kerviel, A. Thomas, L. Chaloin, C. Favard and D. Muriaux, *Virus Res.*, 2013, **171**, 332–340.
- 20 41 J. He, E. Sun, M. V. Bujny, D. Kim, M. W. Davidson and X. Zhuang, *PLoS Pathog.*, 2013, **9**, e1003701.
- 42 X. A. Zhang and C. Huang, *Cell. Mol. Life Sci.*, 2012, **69**, 2843–2852.
- 25 43 Z. Andreu and M. Yáñez-Mó, *Front. Immunol.*, 2014, **5**, 442.
- 44 K. E. Runge, J. E. Evans, Z.-Y. He, S. Gupta, K. L. McDonald, H. Stahlberg, P. Primakoff and D. G. Myles, *Dev. Biol.*, 2007, **304**, 317–325.
- 30 45 S. Charrin, M. Latil, S. Soave, A. Poleskaya, F. Chrétien, C. Boucheix and E. Rubinstein, *Nat. Commun.*, 2013, **4**, 1674.
- 46 J. C. Stachowiak, C. C. Hayden and D. Y. Sasaki, *Proc. Natl. Acad. Sci. U. S. A.*, 2010, **107**, 7781–7786.
- 35 47 J. C. Stachowiak, E. M. Schmid, C. J. Ryan, H. S. Ann, D. Y. Sasaki, M. B. Sherman, P. L. Geissler, D. A. Fletcher and C. C. Hayden, *Nat. Cell Biol.*, 2012, **14**, 944–949.
- 40 48 M. R. Tardif and M. J. Tremblay, *J. Virol.*, 2005, **79**, 4316–4328.
- 49 V. Rocha-Perugini, H. Suárez, S. Álvarez, S. López-Martín, G. M. Lenzi, F. Vences-Catalán, S. Levy, B. Kim, M. A. Muñoz-Fernández, F. Sánchez-Madrid and M. Yáñez-Mó, *Nat. Microbiol.*, 2017, **2**, 1513–1522.
- 45 50 N. Jouvenet, P. D. Bieniasz and S. M. Simon, *Nature*, 2008, **454**, 236–240.
- 51 S. J. D. Neil, T. Zang and P. D. Bieniasz, *Nature*, 2008, **451**, 425–430.
- 50 52 S. Ivanchenko, W. J. Godinez, M. Lampe, H.-G. Kräusslich, R. Eils, K. Rohr, C. Bräuchle, B. Müller and D. C. Lamb, *PLoS Pathog.*, 2009, **5**, e1000652.
- 53 N. Jouvenet, M. Zhadina, P. D. Bieniasz and S. M. Simon, *Nat. Cell Biol.*, 2011, **13**, 394–401.
- 55